Core-level photoelectron spectroscopy from individual heteroepitaxial nanocrystals on GaAs(001)

S. Heun,[1,*] Y. Watanabe,[2] B. Ressel,[1] D. Bottomley,[2] Th. Schmidt,[1,†] and K. C. Prince[1]
[1]*Sincrotrone Trieste, Basovizza, 34012 Trieste, Italy*
[2]*NTT Basic Research Laboratories, Atsugi, Kanagawa 243-01, Japan*
(Received 26 September 2000; published 13 March 2001)

Core-level spectra of individual heteroepitaxial nanocrystals were measured with a spectroscopic photoemission and low-energy electron microscope that allows laterally resolved photoemission spectroscopy. The nanocrystals were obtained by depositing nominally 2 monolayers (ML) of InAs on a Se-terminated GaAs(001) surface. The Se-termination of GaAs results in the formation of a 2–3-ML-thick film of Ga_2Se_3 on top of bulk GaAs. During heteroepitaxy the InAs reacts with the Ga_2Se_3: A phase separation takes place on the anion sublattice, while an alloying takes place on the cation sublattice. During the initial stages of growth, a submonolayer-thick wetting layer of $In_xGa_{1-x}As$ is formed that is covered by $(In_yGa_{1-y})_2Se_3$. $(In_yGa_{1-y})_2Se_3$-covered InAs nanocrystals are formed on this surface.

DOI: 10.1103/PhysRevB.63.125335 PACS number(s): 79.60.Jv, 07.85.Qe, 85.35.Be

I. INTRODUCTION

Strained-layer epitaxial growth results in the spontaneous formation of islands through the Stranski-Krastanov growth mode,[1,2] and because of their quasi-zero-dimensional nature, the islands are often referred to as quantum dots. These quantum dots have attracted considerable attention and may have optical and memory applications.[3,4] Since the islands are formed without lithography, cost-effective fabrication of devices with very small dimensions is envisioned.

However, while the quantum dot concept sounds very promising, there are some serious problems that limit its possibilities. Applications will clearly depend on the control of the quality, composition, size, and uniformity of the dots. For example, size fluctuations lead to a large inhomogeneous broadening of the photoluminescence spectra of ensembles of dots.[5] To overcome this problem, nanoscale spectroscopic techniques have been developed that permit the study of the properties of individual quantum dots.[6]

Another key parameter is the elemental composition of the dots. Segregation and interdiffusion have been observed in the technologically important cases of Ge/Si (lattice mismatch 4%) and InAs/GaAs (lattice mismatch 7%).[7–9] Since these effects are potentially detrimental to device performance, the elemental composition of the quantum dots has to be determined.

When InAs is deposited on a GaAs(001) surface, the growth starts in a two-dimensional layer-by-layer mode. Once a critical amount (about 1.7 monolayers[9]) of InAs is deposited, InAs islands nucleate at the surface. On the other hand, one of us (Y.W.) has shown that the growth of InAs on Se-terminated GaAs leads to the formation of nanocrystals essentially without the formation of a wetting layer.[10] However, the role of the surface termination of GaAs on the nucleation process of InAs quantum dots is still an open issue and under investigation.[11–14]

In this paper we investigate the elemental composition of nanocrystals obtained by heteroepitaxy of InAs on the Se-terminated GaAs surface using a spectroscopic photoemission and low-energy electron microscope (SPELEEM) at the synchrotron radiation source ELETTRA in Trieste, Italy. The Se treatment of the GaAs(001) surface results in a Ga-rich 2–3-ML-thick Ga_2Se_3 film on top of bulk GaAs,[15] with a structure that can be considered to be a variant of the zinc-blende structure with ordered Ga vacancies.[16] Important parameters of the GaAs, InAs, and Ga_2Se_3 crystals are summarized in Table I. Using the high lateral resolution of our microscope in combination with the well-known chemical sensitivity of photoelectron spectroscopy, we were able to obtain spectra from individual nanocrystals and deduce their elemental composition.

II. EXPERIMENT

The nanocrystals were grown by molecular beam epitaxy in Tsukuba, Japan, on a Si-doped *n*-type GaAs(001) wafer with a carrier density of $1\times10^{18}\,cm^{-3}$. A GaAs buffer layer was grown at 500 °C on the GaAs wafer. Then the sample was exposed at 400 °C for 5 min to a Se-beam flux, resulting in a Se-terminated GaAs surface with 2×1 reconstruction. Epitaxial growth of nominally 2 ± 0.2 monolayers (ML) of InAs was then performed at 200 °C. After deposition of the InAs, a 2×1 surface reconstruction was observed in reflection high energy electron diffraction (RHEED). Further details on sample preparation are provided in Refs. 10, 17, and 18.

The sample was protected by an amorphous As-cap layer deposited *in situ* for the transfer in air to ELETTRA, where thermal desorption of the cap layer was performed at 380 °C. After this treatment, the sample showed a 2×1 low-energy electron diffraction (LEED) pattern. We verified that the capping/decapping procedure did not alter the electronic properties of such samples.[18] For this purpose we performed integral high-resolution photoelectron spectroscopy. Virtually identical spectra were obtained from a sample before and after a full capping and decapping cycle. No oxidized components could be detected in the core-level peaks of As $3d$, Ga $3d$, and In $4d$. Furthermore, the intensity ratio of the Ga $3d$ peak to the In $4d$ peak was not changed by capping/decapping. These results indicated that the surface stoichiometry of a freshly prepared sample and of a sample after capping and decapping is basically identical.

TABLE I. Material parameters of the compounds discussed in the text. The data for GaAs, InAs, and Ga_2Se_3 are from Ref. 39. The melting point value from In_2Se_3 is from Ref. 16. The lattice constant value for In_2Se_3 is our estimate based on the ratio of values for InAs and GaAs and the value for Ga_2Se_3.

Material	GaAs	InAs	Ga_2Se_3	In_2Se_3
Lattice constant (Å) at room temperature	5.653	6.058	5.429	5.82
Melting point (K)	1510	1215	1020	1163

All measurements presented in this paper were performed with the SPELEEM at ELETTRA. The instrument is based on a standard low-energy electron microscope (LEEM) but is equipped with an imaging energy analyzer and takes advantage of the high brilliance of the third-generation storage ring to perform spectroscopic microscopy with a maximum energy resolution of better than 0.5 eV and a lateral resolution of 25 nm. To increase the signal, for the experiments described here the SPELEEM was operated with an energy resolution of 1.0 eV. Details concerning the beam line and the microscope are given in Refs. 19–21. For our experiments we used photon energies of 52 eV and 121 eV for the In $4d$/Ga $3d$ and Se $3d$ core-level measurements, respectively, to obtain surface-sensitive information (photoelectron mean free path about 6 Å,[22] which means that approximately the topmost four monolayers contribute to the signal).

After the measurements, an approximately 12-ML-thick gold film was deposited on the sample, and the position of the Au $4f_{7/2}$ photoemission peak [binding energy 84.0 eV (Ref. 23)] was used to calibrate the binding energy axis. The absolute accuracy of the binding energy calibration was estimated to be ± 200 meV.

Apart from x-ray photoemission electron microscopy (XPEEM) we used the SPELEEM to perform spectroscopy in different ways. Integral spectra from the field of view of the microscope (i.e., the diameter of the image, here 2 μm, which corresponds approximately to a 3-μm^2 area) were obtained by measuring the photocurrent of the SPELEEM phosphor screen as a function of photoelectron kinetic energy.[18] Laterally resolved spectra were obtained from a stack of XPEEM images by integration of a selected area.[19] The selected areas described in this paper are the substrate and the nanocrystals, where the ''substrate'' refers to the area of the sample not covered by nanocrystals. Substrate spectra were taken from a 0.01–0.04-μm^2 area well separated from the nanocrystals. It was verified that there was no significant lateral inhomogeneity of the substrate, i.e., spectra taken from different substrate regions were mutually consistent. Nanocrystal spectra were taken from individual objects: the nanocrystal circumference was determined, the outermost pixels of the nanocrystal were discarded (1 pixel corresponds to a sample area of 4 nm×4 nm), and all remaining pixels inside the circumference contributed to the spectrum. Since, within statistical fluctuations, all nanocrystal core-level spectra appeared to be identical, the nanocrystal spectra presented in this paper are all averages over a large number of individual nanocrystals.

Spectra were fitted using Voigt functions and a quadratic background. The peak energy separation Δ_{so} between the spin orbit components was kept constant at 0.45 eV for Ga $3d$,[17,24] 0.85 eV for In $4d$,[25] and 0.86 eV for Se $3d$.[15,26] Their branching ratio was kept constant at 1.5 for all peaks.

III. THEORY

The interpretation of laterally resolved spectra has to take account of the topography of the sample. The synchrotron light illuminates the sample at an angle α from grazing incidence. In our setup, $\alpha = 16°$. Therefore, on a flat sample a circular x-ray beam of diameter d is illuminating an elliptical area of diameter $d_s = d/\sin\alpha$ in the direction of the propagation of the light projected onto the surface plane, and of diameter d in the perpendicular direction in the surface plane. This is illustrated in Fig. 1. However, if the surface of an object on the sample, for example, a nanocrystal, is inclined towards the beam, the size of the illuminated area changes. The diameter of the beam in the direction of the propagation of the light is then $d_f = d/\sin(\beta_f + \alpha)$ with β_f the inclination angle of the object (see Fig. 1). Therefore, with increasing angle β_f the illuminated area decreases as $A_f/A_s = d_f/d_s$. Since the number of photons per second in the incoming beam of diameter d is the same for flat and inclined parts of the sample, the photon flux density on the inclined object's surface increases with β_f as $\Phi_f/\Phi_s = (A_f/A_s)^{-1} = d_s/d_f$, resulting in a higher photoelectron yield from the inclined object. However, the photoelectron

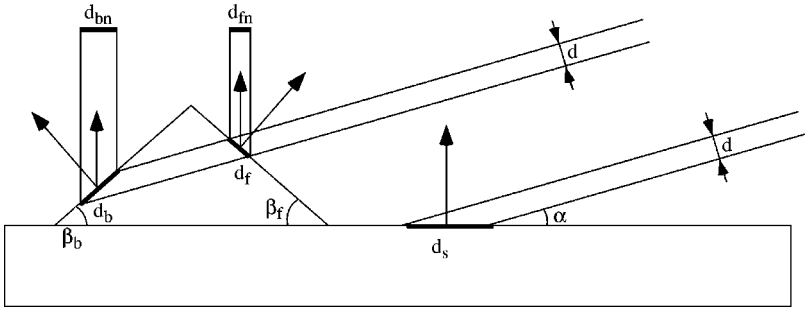

FIG. 1. Sketch of the geometry of the sample.

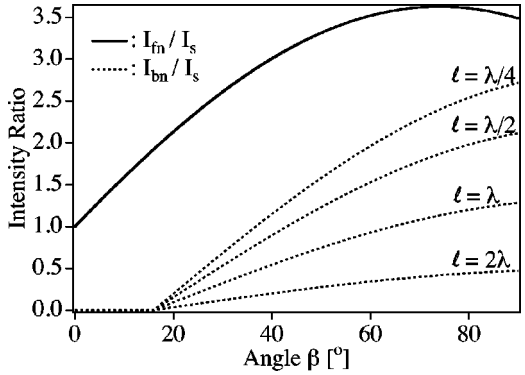

FIG. 2. Relative photoelectron intensity enhancement I_{fn}/I_s (solid line) due to the inclination of the surface of objects on the sample surface as a function of inclination angle β_f for an angle of illumination $\alpha=16°$. The figure shows also the relative photoelectron intensity I_{bn}/I_s (hatched line) from the backside of the inclined objects as a function of inclination angle β_b for $\alpha=16°$ and its dependence on the parameter l/λ. For details, see Fig. 1 and text.

emission from the inclined object is not normal to the sample surface (see Fig. 1), which is the direction of the detector. This has two implications: (a) To a first approximation, the angular distribution of the photoemitted electrons is $I_f(\beta_f)=I_0\cos\beta_f$.[27] This formula reflects the increasing path length of the photoelectrons in the solid when they leave it under a shallow angle. Therefore the attenuation of the photoelectrons is stronger, and less atomic layers contribute to the signal. Furthermore, for large angles β_f one has also to consider the differences in probing depth, since the photoelectrons are collected from the flat part of the sample in normal emission (more bulk sensitive), while from the inclined part they are collected at a shallow angle (more surface sensitive). (b) The surface of the object is inclined with respect to the detector. Projected on the detector plane, the illuminated area on the object is $d_{fn}=d_f\cos\beta_f$, i.e., smaller by a factor $\cos\beta_f$ (see Fig. 1). These two contributions actually tend to cancel each other, so that we obtain for emission along the sample normal a photoelectron intensity ratio from inclined to flat unit areas of the sample of

$$\frac{I_{fn}}{I_s}=\frac{\Phi_f}{\Phi_s}=\frac{\sin(\beta_f+\alpha)}{\sin\alpha}. \tag{1}$$

For $\alpha=16°$, this is shown in Fig. 2 as a function of β_f from 0° to 90°. The figure shows that a signal increase by a factor of more than 3 can occur. The curve has its maximum value for $\beta_f=90°-\alpha$, when the light beam is normal to the object's surface.

If the size of the inclined object is small, i.e., comparable to the x-ray attenuation length of the solid, then a significant fraction of the photons can travel through the object and excite photoelectrons at its backside. There the diameter of the light spot is $d_{bn}=d_b\cos\beta_b$ with $d_b=d/\sin(\beta_b-\alpha)$, as illustrated in Fig. 1. Here, the angle β_b gives the inclination of the object's backside with respect to the sample surface. The angular distribution of the photoemitted electrons is the same as at the front of the object ($I_b\propto\cos\beta_b$), but since the light was propagating through the object, its intensity is attenuated exponentially,[28] so that $I_b(\beta_b)=I_0\exp(-l/\lambda)\cos\beta_b$, with l the length of the light path in the object and λ the x-ray attenuation length. This gives a photoelectron intensity ratio per unit area from inclined to flat region for emission along the sample normal of

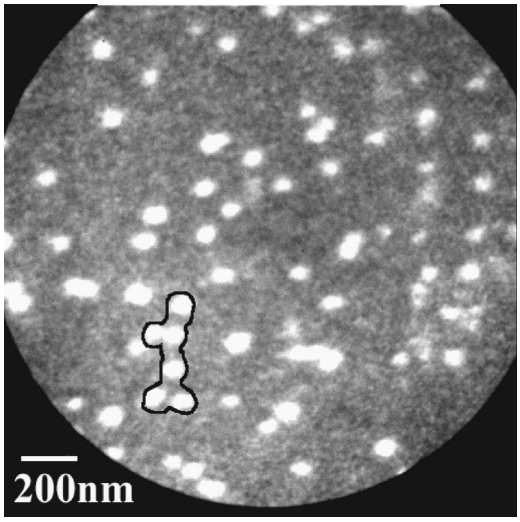

FIG. 3. LEEM image from the sample. Nanocrystals are bright. A characteristic group of nanocrystals is delineated by a boundary drawn in black. The electron energy was 26.5 eV.

$$\frac{I_{bn}}{I_s}=\frac{\Phi_b}{\Phi_s}=\frac{\sin(\beta_b-\alpha)}{\sin\alpha}\ e^{-l/\lambda}. \tag{2}$$

This function is drawn in Fig. 2 for $\alpha=16°$ and for different values of l/λ. Clearly, for $l\gg\lambda$, emission from the backside of the inclined object can be neglected. However, for $l=\lambda$ and large angles β_b the intensity ratio is close to 1, and for $l=\lambda/4$ and large β_b the emission from the backside of the inclined object is twice as strong as the emission from the substrate. For small angles ($\beta_b<\alpha$) the light cannot reach the backside of the object, and consequently no photoelectrons are excited.

IV. RESULTS

Figure 3 shows an electron microscopy (LEEM) image from the sample. It was taken at an electron energy of 26.5 eV. The field of view is 2 μm. A characteristic group of nanocrystals is indicated by a marker. The nanocrystals are clearly resolved as bright spots on a dark substrate.

We performed a statistical analysis of the nanocrystal density and their size distribution. The sampled area was 20 μm^2, and the nanocrystal density was found to be $25\pm4\ \mu m^{-2}=(25\pm4)\times10^8\ cm^{-2}$. A histogram of the nanocrystal size distribution is shown in Fig. 4, and has a maximum for a nanocrystal diameter $\langle d\rangle$ of about 50 nm. The nanocrystal size distribution is clearly skewed. The appearance of nanocrystals with a diameter $d\geqslant2\langle d\rangle$ is mostly due to groups of two or more nanocrystals that are too close together to be resolved individually. Nanocrystals with a diameter smaller than 21 nm could not be resolved. This value agrees with the lateral resolution of the SPELEEM deter-

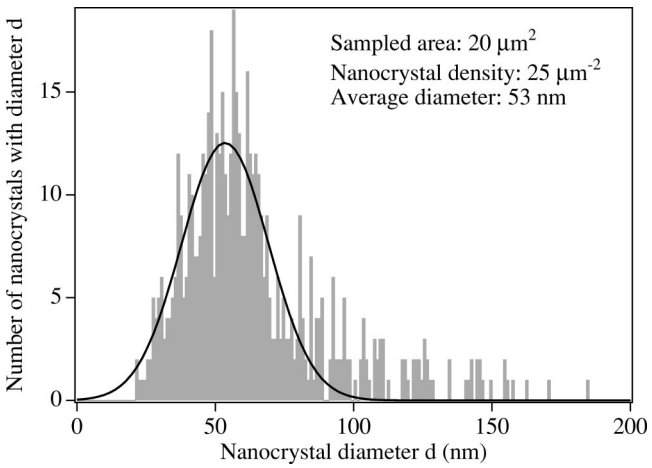

FIG. 4. Histogram of nanocrystal size distribution (bars) with Gaussian fit (solid line). The average nanocrystal diameter is 53 ±16 nm.

mined by a different method as described in Ref. 20. The histogram curve was fitted with a Gaussian function that is also shown in Fig. 4. From this fit we deduce an average nanocrystal diameter of 53±16 nm.

Figure 5 shows XPEEM images of the sample obtained with photoelectrons from (a) the In 4*d* and (b) the Ga 3*d* core level. They were measured with a photon energy of 52.0 eV. The field of view is 2 μm for both images. The contour in the images highlights the same group of nanocrystals as in Fig. 3. In Fig. 5(a), the nanocrystals are clearly evident as bright spots on the substrate. Positive contrast (i.e., bright nanocrystals on dark substrate) is observed for binding energies ranging from 18.6 eV to 15.1 eV, i.e., for all energies for which the emission from the In 4*d* core level is stronger than the emission from the Ga 3*d* core level. Thus, the contrast we observe is pure elemental contrast. In contrast to Fig. 5(a), Fig. 5(b) shows dark features on the substrate. However, these dark features are actually the shadows of the nanocrystals, which explains their elongated shape. The group contour shows that the intensity from nanocrystals and substrate in Fig. 5(b) is equal within our experimental precision, i.e., no contrast between nanocrystals and substrate is observed at the energy of the Ga 3*d* core level. On careful inspection, the shadows of the nanocrystals are also visible in Fig. 5(a). They are caused by the light illuminating the sample at a glancing incidence angle of 16° from the upper right corner of the image. The direction of the incoming beam is indicated by the arrow in Fig. 5(b). From the length of the shadows, we estimate the average height of the nanocrystals to be 22±3 nm.

In Fig. 6 we display spectra obtained from the sample area shown in Fig. 5. Figure 6(a) shows an integral spectrum of the Ga 3*d* and In 4*d* core levels, measured at a photon energy of 52 eV. A peak shape analysis of this spectrum was performed as described in Sec. II, and the result is also shown in Fig. 6(a). Figure 6(b) shows laterally resolved photoelectron spectra from the nanocrystals and from the substrate, measured at a photon energy of 52 eV. The spectra were obtained from a stack of XPEEM images, two examples of which are shown in Fig. 5. The main features of the two spectra agree with the integral spectrum depicted in Fig. 6(a). The apparent shift between the spectra in Figs. 6(a) and 6(b) is within the uncertainty of the binding energy calibration. The two spectra in Fig. 6(b) show a clear difference between nanocrystals and substrate in the photoelectron yield from the In 4*d* core level. In fact, the In 4*d* core level emission intensity from the substrate is only (62±3)% of the emission intensity from the nanocrystals. This explains the strong contrast observed in Fig. 5(a). On the other hand, the photoelectron yields from the Ga 3*d* core level from nanocrystals and substrate are equal. This is in agreement with the vanishing contrast in Fig. 5(b). Figure 6(b) shows that the main contrast mechanism in the images in Fig. 5 is a higher

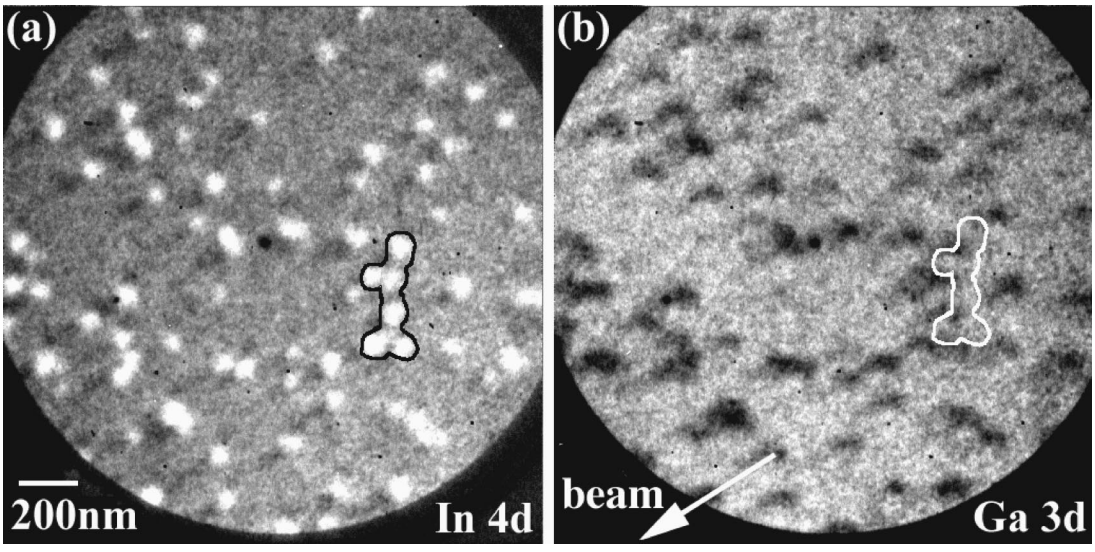

FIG. 5. XPEEM images using (a) the In 4*d* core level (photoelectron binding energy E_b=17.4 eV) and (b) using the Ga 3*d* core level (E_b=20.1 eV). The photon energy was $h\nu$=52 eV. The contour indicates the same group of nanocrystals as in Fig. 3. The direction of the incoming light beam is indicated by the arrow in (b).

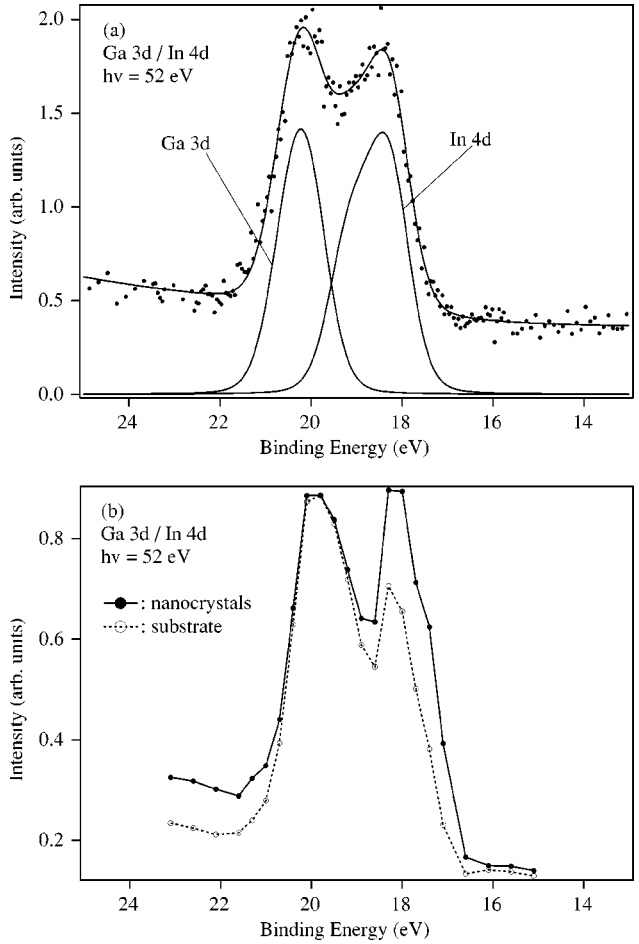

FIG. 6. Ga 3*d* and In 4*d* core level photoelectron spectra. The photon energy was 52 eV. (a) Integral measurement from a 3-μm^2 area. Dots: data points, full line: fit. The result of the fit with the background subtracted is also shown below the data. (b) Laterally resolved data of nanocrystals (●) and substrate (○).

In content in the nanocrystals with respect to the substrate.

Figure 7 shows an XPEEM image measured at a binding energy of 54.7 eV, i.e., at the Se 3d core level emission. It was obtained with a photon energy of 121 eV. Figure 7 looks like the inversion of Fig. 5(a) in that it shows dark nanocrystals on the substrate. This contrast is observed for binding energies from 56.5 eV to 52.9 eV, i.e., for energies for which the emission is predominantly from the Se 3*d* core level. The marker in the image highlights the same group of nanocrystals as in Figs. 3 and 5, so we are sure that all measurements discussed in this paper were obtained from the same sample area.

For the Se 3*d* core level, we measured photoelectron spectra from the same sample area mentioned above, Fig. 8, at a photon energy of 121 eV. Figure 8(a) shows an integral photoelectron spectrum measured *in situ* with the SPELEEM. The core level was fitted by two doublets that are separated by 1.0 eV. Due to the moderate energy resolution the SPELEEM was operated with, the doublets are not clearly resolved. The intensity ratio between the doublet at higher binding energy, labeled A in Fig. 8(a), and the doublet at lower binding energy, labeled B, is $I_A/I_B = 2.26 \pm 0.07$.

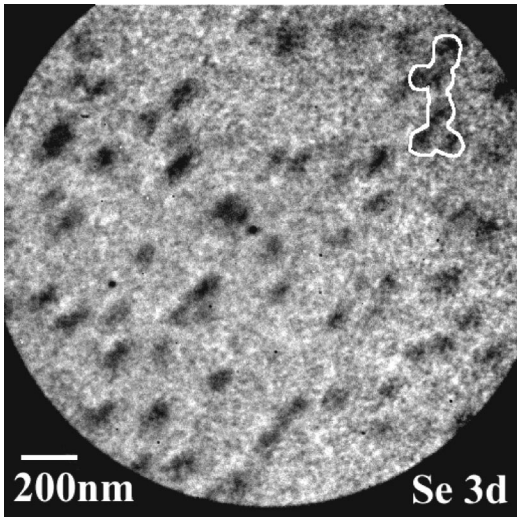

FIG. 7. XPEEM image using the Se 3*d* core level (photon energy $h\nu = 121$ eV, photoelectron binding energy $E_b = 54.7$ eV). The white boundary line indicates the same group of nanocrystals as in Figs. 3 and 5.

Figure 8 (b) shows laterally resolved spectra from the nanocrystals, the substrate, and an area of 1 μm^2 including nanocrystals and substrate (integral spectrum). The photoelectron yield from the nanocrystals amounts to 72% of the photoelectron yield from the substrate. This explains the contrast observed in Fig. 7. Apart from the peak intensity, both spectra are mutually consistent. They are also very similar to the integral spectra shown in Figs. 8(a) and 8(b). Therefore we conclude that the contrast in Fig. 7 is only due to a higher Se concentration at the surface of the substrate as compared to the surface of the nanocrystals.

V. DISCUSSION

The peak shape analysis of the integral spectra in Figs. 6(a) and 8(a) allows a comparison with literature data that were obtained with high-resolution integral photoelectron spectroscopy. The Ga 3*d* and In 4*d* core levels were each fitted with one spin-orbit split doublet. Taking into account the moderate-energy resolution the SPELEEM was operated with, these spectra are in good agreement with literature data.[10,17,29] A possible chemical shift between In or Ga bonding to As or Se could not be resolved, because it was only observed in experiments with an energy resolution better than 0.3 eV.[10,17] In Fig. 8(a), the Se 3*d* core level was fitted with two doublets separated by 1.0 eV. This is in agreement with a communication that the Se 3*d* core level peak of Se-terminated GaAs is composed of two doublets corresponding to two different Se chemical states, and whose energy separation ranges from 0.97 eV to 1.00 eV.[15] Equally good agreement was obtained for the As 3*d* core level (not shown here).[30] In summary, the integral spectra that we measured are consistent with high-resolution photoelectron spectroscopy data obtained from in situ grown samples. This allows us to draw two conclusions:

(1) The sample used for the SPELEEM investigations had the same electronic structure as samples analyzed directly

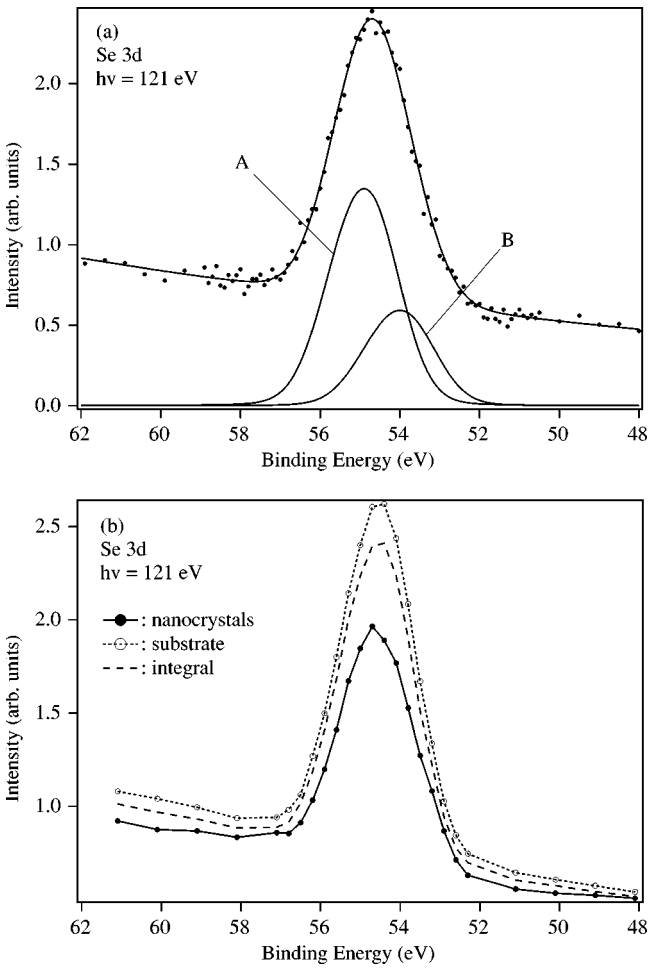

FIG. 8. Se 3*d* core-level photoelectron spectra. Photon energy: 121 eV. (a) Integral measurement from a 3-μm^2 area. Dots: data points, full line: fit. The result of the fit with the background subtracted is also shown below the data. (b) Laterally resolved data from nanocrystals (●) and substrate (○). An integral spectrum (obtained from a 1-μm^2 sample area including nanocrystals and substrate) is also shown for comparison.

after growth in a conventional molecular beam epitaxy system. In particular, the capping and decapping protocol employed to protect the samples during transfer in air did not change the electronic structure of the sample.[18] Furthermore, the surface reconstruction and the sample morphology were not changed significantly by the capping and decapping procedure, as described in Sec. II and demonstrated in Figs. 3 and 4.

(2) Photoelectron spectroscopy with the SPELEEM is a reliable way to obtain information on the electronic structure of a sample from a micrometer-sized area. Other examples where the SPELEEM has been successfully employed to obtain spectra from μm-scale objects include Pb islands on Si,[20] lateral inhomogeneities in Schottky barriers,[31] a field-effect transistor,[19] and liquid Au-Si droplets.[32]

The spectra shown in Figs. 6 and 8 allow a deeper understanding of the XPEEM images shown in Figs. 5 and 7. While the images might suggest a simple picture of the sample—InAs nanocrystals on a Se-terminated GaAs surface—the spectra indicate that such a model is an oversimplification. We clearly observed on the one hand an In 4*d* signal from the substrate and on the other hand a Se 3*d* signal from the nanocrystals. Furthermore, the Ga 3*d* signals from the nanocrystals and the substrate are equal within our experimental resolution. Consequently, the sample does not correspond to the simple picture, but interdiffusion and segregation have taken place.

In order to apply the topographic correction to the laterally resolved spectra (as discussed in Sec. III), we need to know the shape and orientation of the nanocrystals. With high-resolution LEEM we determined that the nanocrystals have approximately a square base oriented along the $\langle 110 \rangle$ directions of the surface.[30] From high-resolution scanning electron microscopy and cross-sectional transmission electron microscopy we know that they grow with a truncated pyramidal shape,[10,33] and from *in situ* RHEED we deduce that the pyramid sides are composed of {111} facets.[10] This implies that the nanocrystal edges are along the $\langle 110 \rangle$ directions, which is consistent with the LEEM result. The angle between (001) and {111} planes is 54.7°, which gives according to the Appendix an intensity correction factor of 1.75. In the experimental geometry, the pyramid base edges were rotated 45° with respect to the beam: the projection of the light propagation direction onto the surface was along a $\langle 100 \rangle$ direction. Therefore, the illuminated area is enlarged by a factor of $\sqrt{2}$ and the correction factor is reduced to 1.24.

When corrected for geometrical effects, the intensity in the In 4*d* emission from the substrate amounts to (77 $\pm$4)% of the intensity of the emission from the nanocrystals. Therefore, InAs grows on Se-terminated GaAs(001) in a mode similar to the Stranski-Krastanov (SK) growth mode and not in the Volmer-Weber mode.[9] In fact, the critical thickness of the InAs wetting layer on the Se/GaAs substrate has been determined to be somewhat less than 1 ML.[17] Even though the reconstruction of the Se-terminated GaAs surface remains unchanged upon InAs deposition, there is further evidence from high-resolution photoemission spectroscopy that at least part of the substrate surface is covered by In atoms that bond to Se atoms.[10]

The laterally resolved Se 3*d* core-level spectra show a Se signal not only from the Se-terminated GaAs surface but also from the nanocrystals. Therefore, a substantial amount of Se atoms are present at the nanocrystals' surfaces. From the valence band and the work function value of this sample there is further evidence for the presence of Se at the surface of the nanocrystals.[30] A similar observation is made at the Ga 3*d* core level. We clearly observe a Ga 3*d* core-level emission from the nanocrystals, indicating a substantial amount of Ga at the surface of the nanocrystals. Corrected for the topography, the Ga 3*d* core-level intensity from the nanocrystals is 92% of the intensity from the substrate surface (including the wetting layer).

The *A* component in the Se 3*d* core level shown in Fig. 8(a) was assigned to Se atoms that have no Ga vacancy as a nearest neighbor, while the *B* component corresponds to Se atoms that have one Ga vacancy as a nearest neighbor.[15] The *B* component species are located nearer to the surface than the *A* component species. The intensity ratio I_A/I_B for Se-

terminated GaAs(001) for normal emission and at photon energy $h\nu = 130$ eV has been determined to be 1.51.[15] After deposition of 2 ML of InAs, at a photon energy of 121 eV we measured an intensity ratio I_A/I_B of 2.26, also for normal emission. Since neither the mean free path nor the photoionization cross section for the Se $3d$ core level at these photon energies changes strongly, we can conclude that after the deposition of 2 ML of InAs on Se-terminated GaAs, the population of the B species relative to the A species is decreased compared to the pristine Se-terminated GaAs surface.

The average nanocrystal diameter and height are $d = 53$ nm and $h = 22$ nm, respectively, and their mean density is $25\,\mu\text{m}^{-2}$. Quantitative information regarding the volume of the nanocrystals can be obtained from the measured dimensions. The volume of the nanocrystals was obtained from $hA/2$, with $A = \pi d^2/4$ being the area of the base of each nanocrystal.[34] This gives an approximate nanocrystal volume per μm^2 of $6\times10^5\,\text{nm}^3$. The total volume of deposited InAs is 2 ML = 0.6 nm, corresponding to $6\times10^5\,\text{nm}^3$ per μm^2. However, we know that the InAs grows in a mode similar to the SK mode. Therefore, part of the InAs was consumed in the wetting layer and is not available for the nanocrystals. Consequently, the nanocrystals have a greater volume than expected from this simple calculation, and the implication is that the additional material must have been provided by another source, i.e., the Ga_2Se_3.

Since the growth temperature of our sample was 200 °C, and we know that to a good approximation InAs and GaAs do not alloy at this temperature,[9] we can consider the GaAs substrate to be inert. However, our measurement of the Se $3d$ core level provides evidence that a reaction between InAs and Ga_2Se_3 has taken place upon InAs deposition. The formation of a quaternary compound containing In, Ga, Se, and As is not very likely because the anion species (As and Se) are unlikely to alloy substantially since they are from different chemical groups (V and VI, respectively). On the cation sublattice (In and Ga), some alloying is more likely. There is a clear energetic advantage for some Ga to go from Ga_2Se_3 into the InAs, and for In to go from InAs to Ga_2Se_3. The reason is minimizing the strain with respect to the GaAs substrate. Ga_2Se_3 is under 4.1% tensile strain on GaAs. If In goes into the Ga_2Se_3, forming some In_2Se_3, the magnitude of the strain will be reduced. Similarly when Ga goes into the InAs, the magnitude of the strain in the wetting layer with respect to the substrate is reduced. However, it is unlikely that the InAs nanocrystals have bulk inclusions of Ga_2Se_3 because of the 10% lattice mismatch between the two. The picture that emerges is that the surface layers of the substrate and the nanocrystals are two-dimensional domains of $In_xGa_{1-x}As$ and $(In_yGa_{1-y})_2Se_3$, with little alloying occurring on the anion sublattice. Such phase separation on the anion sublattice most probably due in part to a miscibility gap has indeed been observed for $InAs_xSb_{1-x}$ and for $GaAs_ySb_{1-y}$ epitaxial films.[35–38]

This model is consistent with the fact that we observe an In $4d$, a Ga $3d$, and a Se $3d$ signal from both the nanocrystals and the wetting layer. It is also consistent with our observation that there is a higher In $4d$ signal from the nanocrystals than from the wetting layer, and (after correction for sample topography) a higher Ga $3d$ signal from the substrate than from the nanocrystals. Furthermore, it agrees with our observation that some Se atoms are removed from the Ga_2Se_3-terminated surface upon InAs deposition, and with the observed nanocrystal volume being larger than can be accounted for if alloying processes were neglected.

VI. CONCLUSION

In summary, we observed the elemental composition of nanocrystals and the surrounding substrate surface by laterally resolved core-level spectroscopy. During the deposition of InAs on Se-terminated GaAs, the InAs reacts with the Ga_2Se_3: A phase separation takes place on the anion sublattice, while an alloying takes place on the cation sublattice. During the initial stages of growth, a submonolayer-thick wetting layer of $In_xGa_{1-x}As$ is formed that is covered by $(In_yGa_{1-y})_2Se_3$. $(In_yGa_{1-y})_2Se_3$-covered InAs nanocrystals are formed on this surface. The implication of our results is that significant mass transport has occurred from the Se-terminated GaAs surface to the nanocrystals. Under such complicated circumstances the SPELEEM has proven to be a powerful instrument for spectromicroscopy on technologically relevant sub-100-nm structures.

ACKNOWLEDGMENTS

Helpful discussions with Lucia Sorba and F. Maeda are gratefully acknowledged, as is the assistance of M. Lazzarino during the measurements. This work was performed with the SPELEEM microscope of the Technical University of Clausthal. Th.S. acknowledges support from the European Union under Contract No. ERBFMBICT961749. We thank Professor E. Bauer for his encouragement.

APPENDIX: CALCULATION OF THE TOPOGRAPHIC CORRECTION

To calculate the intensity correction factor for the nanocrystals according to Sec. III, we need to split the nanocrystals into front side, top, and backside. The inclination angle is $\beta_f = \beta_b = 54.7°$, the average height of the nanocrystals 22 nm, and therefore the base length of the front side is $22\,\text{nm}/\tan 54.7° = 16\,\text{nm}$. The same holds for the backside. The average nanocrystal diameter is 53 nm; therefore their base length is $53\,\text{nm}/\sqrt{2} = 37\,\text{nm}$, so that the flat top of the nanocrystals has an extension of $37\,\text{nm} - (2\times16\,\text{nm}) = 5$ nm. According to Eq. (1), the intensity correction factor for the front side for $\beta_f = 54.7°$ is 3.42. The x-ray attenuation length of InAs at a photon energy of 50 eV is approximately 20 nm,[28] so in Eq. (2) we have $l \approx 2\lambda$, and therefore the intensity correction factor for the backside of the nanocrystals is 0.31. The resulting correction factor for the nanocrystals is the weighted average of these values. It is obtained from $[(16\,\text{nm}\times3.42) + (5\,\text{nm}\times1.0) + (16\,\text{nm}\times0.31)]/37\,\text{nm} = 1.75$.

*Corresponding author. FAX: +39-040-375-8565; Email: stefan.heun@elettra.trieste.it

†Present address: Experimentelle Physik II, Universität Würzburg, Germany.

[1] R. Nötzel, J. Temmyo, and T. Tamamura, Nature (London) **369**, 131 (1994).

[2] G. Springholz, V. Holy, M. Pinczolits, and G. Bauer, Science **282**, 734 (1998).

[3] J. J. Finley, M. Skalitz, M. Arzberger, A. Zrenner, G. Böhm, and G. Abstreiter, Appl. Phys. Lett. **73**, 2618 (1998).

[4] H. Sakaki, Surf. Sci. **267**, 623 (1992).

[5] J.-Y. Marzin, J.-M. Gérard, A. Izraël, D. Barrier, and G. Bastard, Phys. Rev. Lett. **73**, 716 (1994).

[6] Y. Toda, M. Kourogi, M. Ohtsu, Y. Nagamune, and Y. Arakawa, Appl. Phys. Lett. **69**, 827 (1996).

[7] D. J. Bottomley, Jpn. J. Appl. Phys., Part 2 **36**, L1464 (1997); Appl. Phys. Lett. **72**, 783 (1998); J. Vac. Sci. Technol. B **17**, 259 (1999).

[8] T. I. Kamins, G. Medeiros-Ribeiro, D. A. A. Ohlberg, and R. S. Williams, J. Appl. Phys. **85**, 1159 (1999).

[9] P. B. Joyce, T. Krzyzewski, G. R. Bell, B. A. Joyce, and T. S. Jones, Phys. Rev. B **58**, R15 981 (1998).

[10] Y. Watanabe, F. Maeda, and M. Oshima, in *Proceedings of the Twenty-First International Symposium on Compound Semiconductors*, San Diego, CA, September 1994, edited by Herb Goronkin and Umesh Mishra, Institute of Physics Conf. Ser. 141 (IOP, Bristol, 1995), Chap. 2, p. 143.

[11] G. A. M. Safar, W. N. Rodrigues, L. A. Cury, H. Chacham, M. V. B. Moreira, S. L. S. Freire, and A. G. de Oliveira, Appl. Phys. Lett. **71**, 521 (1997).

[12] B. R. A. Neves, M. S. Andrade, W. N. Rodrigues, G. A. M. Safar, M. V. B. Moreira, and A. G. de Oliveira, Appl. Phys. Lett. **72**, 1712 (1998).

[13] Y. Watanabe, T. Scimeca, F. Maeda, and M. Oshima, Jpn. J. Appl. Phys., Part 1 **33**, 698 (1994).

[14] Y. Watanabe, F. Maeda, and M. Oshima, Appl. Phys. Lett. **82/83**, 136 (1994).

[15] F. Maeda, Y. Watanabe, T. Scimeca, and M. Oshima, Phys. Rev. B **48**, 4956 (1993).

[16] *Semiconductors-Basic Data*, edited by O. Madelung (Springer, Berlin, 1996).

[17] Y. Watanabe, F. Maeda, and M. Oshima, J. Electron Spectrosc. Relat. Phenom. **80**, 221 (1996).

[18] Y. Watanabe, S. Heun, Th. Schmidt, and K. C. Prince, Jpn. J. Appl. Phys., Suppl. **38**, 556 (1999).

[19] S. Heun, Th. Schmidt, B. Ressel, E. Bauer, and K. C. Prince, Synchrotron Radiat. News **12**, 25 (1999).

[20] Th. Schmidt, S. Heun, J. Slezak, J. Diaz, K. C. Prince, G. Lilienkamp, and E. Bauer, Surf. Rev. Lett. **5**, 1287 (1998).

[21] Th. Schmidt, J. Slezak, S. Heun, J. Diaz, R. R. Blyth, R. Delaunay, D. Cocco, K. C. Prince, E. Bauer, and M. Coreno, J. Synchrotron Radiat. **6**, 957 (1999).

[22] M. P. Seah and W. A. Dench, Surf. Interface Anal. **1**, 2 (1979).

[23] J. F. Moulder, W. F. Stickle, P. E. Sobol, K. D. Bomben, and J. Chastain, *Handbook of X-Ray Photoemission Spectroscopy* (Perkin-Elmer, Eden-Prairie, Minnesota, 1992).

[24] G. Le Lay, D. Mao, A. Kahn. Y. Hwu, and G. Margaritondo, Phys. Rev. B **43**, 14 301 (1991).

[25] Y. Watanabe and F. Maeda, Appl. Surf. Sci. **117/118**, 735 (1997).

[26] S. Takatani, T. Kikawa, and M. Nakazawa, Phys. Rev. B **45**, 8498 (1992).

[27] G. Pirug, A. Winkler, and H. P. Bonzel, Surf. Sci. **163**, 153 (1985).

[28] http://www-cxro.lbl.gov/optical_constants/atten2.html

[29] Y. Watanabe, F. Maeda, and M. Oshima (unpublished).

[30] S. Heun, Y. Watanabe, B. Ressel, Th. Schmidt, and K. C. Prince (unpublished).

[31] S. Heun, T. Schmidt, J. Slezak, J. Diaz, K. C. Prince, B. H. Müller, and A. Franciosi, J. Cryst. Growth **201/202**, 795 (1999).

[32] B. Ressel, S. Heun, Th. Schmidt, and K. C. Prince, Defect Diffus. Forum **183-185**, 181 (2000).

[33] Y. Watanabe and F. Maeda, Appl. Surf. Sci. **162-163**, 625 (2000).

[34] Joyce *et al.* (Ref. 9) compared different expressions used to estimate the nanocrystal volume V (planoconvex and pyramidal shape) and found negligible differences. They proposed to use the expression $V=hA/2$.

[35] I. T. Ferguson, A. G. Norman, B. A. Joyce, T.-Y. Seong, G. R. Booker, R. H. Thomas, C. C. Phillips, and R. A. Stradling, Appl. Phys. Lett. **59**, 3324 (1991).

[36] A. G. Norman, T.-Y. Seong, I. T. Ferguson, G. R. Booker, and B. A. Joyce, Semicond. Sci. Technol. **8**, S9 (1993).

[37] T.-Y. Seong, A. G. Norman, I. T. Ferguson, and G. R. Booker, J. Appl. Phys. **73**, 8227 (1993).

[38] I. T. Ferguson, A. G. Norman, and T.-Y. Seong, J. Appl. Phys. **88**, 5733 (2000).

[39] *Handbook of Physics and Chemistry*, 79th ed., edited by D. R. Lide (CRC Press, Boca Raton, 1998), p. 12–94.